Measurement of the ^{27}Al$(p,\alpha)^{24}$Mg fusion reaction at astrophysical energies via the Trojan Horse Method.

M. La Cognata[1,*], *S.* Palmerini[2,3], *P.* Adsley[4,5], *F.* Hammache[6], *A.* Di Pietro[1], *P.* Figuera[1], *F.* Dell ' Agli[7], *R.* Alba[1], *S.* Cherubini[1,8], *G.L.* Guardo[1], *M.* Gulino[1,9], *L.* Lamia[1,8,10], *D.* Lattuada[1,9], *C.* Maiolino[1], *A.* Oliva[1,8], *R.G.* Pizzone[1], *P.* Prajapati[1,11], *G.G.* Rapisarda[1,8], *S.* Romano[1,8,10], *D.* Santonocito[1], *R.* Spartà[1,8], *M.L.* Sergi[1,8], *A.* Tumino[1,9], and *P.* Ventura[7]

[1]Istituto Nazionale di Fisica Nucleare, Laboratori Nazionali del Sud, 95123 Catania, Italy
[2]Dipartimento di Fisica e Geologia, Università degli Studi di Perugia, 06123 Perugia, Italy
[3]Istituto Nazionale di Fisica Nucleare, Sezione di Perugia, 06123 Perugia, Italy
[4]iThemba Laboratory for Accelerator Based Sciences, Somerset West 7129, South Africa
[5]Cyclotron Institute and Department of Physics & Astronomy, Texas A&M University, College Station, Texas 77843-4242, USA
[6]Institut de Physique Nucléaire d'Orsay, UMR8608, IN2P3-CNRS, Université Paris Sud 11, 91406 Orsay, France
[7]INAF, Observatory of Rome, Monte Porzio Catone (RM), 00077, Italy
[8]Dipartimento di Fisica e Astronomia " Ettore Majorana ", Università degli Studi di Catania, 95123 Catania, Italy
[9]Facoltà di Ingegneria e Architettura, Università degli Studi " Kore ", 94100 Enna, Italy
[10]CSFNSM-Centro Siciliano di Fisica Nucleare e Struttura della Materia, 95123 Catania, Italy
[11]Manipal Centre for Natural Sciences, MAHE, Manipal - 576104, India

Abstract. In astrophysics, the abundance of ^{26}Al is essential for understanding nucleosynthesis in the Milky Way and Galactic core-collapse supernovae rates. Detection methods involve γ-ray lines and comparing ^{26}Mg overabundance with the common Mg isotope in meteorites. Therefore, stable isotopes ^{27}Al and ^{24}Mg play a crucial role and the MgAl cycle affecting aluminum and magnesium production has to be carefully studied. Recent surveys reveal complexities in stellar populations whose understanding may also benefit from better constraining the closure of the MgAl cycle. The ^{27}Al$(p,\alpha)^{24}$Mg fusion reaction, a key ^{27}Al destruction channel, is central to these scenarios. Due to uncertainties, the Trojan Horse Method is applied, allowing high-precision spectroscopy on the compound nucleus ^{28}Si. It reveals crucial fusion cross section information in the astrophysically relevant energy range. The indirect measurement by means of the ^{2}H(^{27}Al,α^{24}Mg)n process made it possible to assess the contribution of the 84.3 keV resonance and to set upper limits on nearby resonances. This study evaluates the THM recommended rate's impact on intermediate-mass asymptotic giant branch stars, showing a notable increase in surface aluminum abundance at lower masses due to fusion cross section modification, while ^{24}Mg remains largely unaffected.

1 Astrophysical background

Measuring Mg and Al isotopic abundances in various astrophysical scenarios plays a very important role. Recent observations, particularly in red-giant-branch stars within globular clusters like NGC 2808, ω-Cen, and M4, have revealed a compelling anti-correlation between Mg and Al abundances. High-resolution stellar spectroscopy has provided evidence for the existence of multiple stellar populations and challenges the conventional understanding of the correlation between Mg isotopes and Al [1, 2].

This intricate observational scenario suggests the involvement of multiple stellar polluters, such as massive fast-rotating stars, intermediate-mass asymptotic giant branch (AGB) stars, and super AGB stars [3]. Theoretical models must be fine-tuned, given the sensitivity of Mg and Al nucleosynthesis to the temperature of stellar H-burning, especially in the narrow temperature range of $0.07 \leq T_9 \leq 0.08$, where T_9 represents the temperature expressed in GK.

The MgAl cycle, occurring in high-temperature H-burning of evolved stars [4], is highlighted for its influence on Mg and Al isotopes nucleosynthesis, despite having higher Coulomb barriers compared to the CNO cycle. Uncertainties in the ^{27}Al$(p,\alpha)^{24}$Mg reaction rate, a common thread in these processes, challenge the reliability of astrophysical predictions [5].

The ^{27}Al$(p,\alpha)^{24}$Mg, involved in the destruction of ^{27}Al, the production of ^{24}Mg, and the closure of the MgAl cycle, competes with the ^{27}Al$(p,\gamma)^{28}$Si reaction. The dominance of the (p,γ) rate above 1 GK and its slight exceedance of the (p,γ) rate in the 0.03-0.08 GK range are highlighted in ref.[6], though uncertainties in these rates underscore the need for a careful assessment of the reaction cross section in the energy range typical of stellar nucleosynthesis, approximately around 100 keV.

The ^{27}Al$(p,\alpha)^{24}$Mg reaction is also involved in understanding the nucleosynthesis of ^{26}Al in our galaxy. The

*e-mail: lacognata@lns.infn.it

presence of ^{26}Al in the Early Solar System is indicated by large excesses of ^{26}Mg measured in presolar grains [7]. Such excesses of ^{26}Mg pointing at ^{26}Al occurrence are quantified with respect to the most abundant Mg isotope (A=24) in meteorites; the precision achieved in isotopic ratio determinations [7] necessitates high-precision investigations of the nucleosynthesis of ^{26}Al, ^{27}Al, and ^{24}Mg.

2 Present status

Even if the ^{27}Al(p,α)^{24}Mg reaction plays a crucial role in astrophysics, one of the widely adopted rates, reported in ref. [9], provides lower, median, and upper values of 1.85×10^{-11}, 4.34×10^{-11}, and 8.51×10^{-11} cm^3 mol^{-1} s^{-1}, respectively, at $T_9 = 0.1$. This range covers almost one order of magnitude, with larger uncertainties at lower temperatures.

The reaction rate in ref.[9] is derived from a combination of direct measurements, compiled spectroscopic data, transfer-reaction-based branching ratios, and shell-model calculations. Direct measurements by ref.[10] explored the low-energy region, setting upper limits for resonance strengths. Spectroscopic data from ref.[17, 18] form the foundation of the calculation, but these datasets lack experimental data focusing on astrophysical energies. Ref.[22] used the ^{27}Al(^{3}He, d)^{28}Si reaction to set upper limits and calculate partial widths and resonance strengths. Shell-model calculations by ref.[19] excluded certain states based on predicted unnatural parity.

With over 90 resonances in the $E_{cm} \leq 3$ MeV region, establishing a reliable reaction rate is challenging. Ref.[16] presented an analysis of available data, leading to deviations from the previous recommended rate in ref.[8]. The main update from 2001 to 2010, resulting in the presently recommended reaction rate in ref.[9], involved an improved approach for calculating uncertainties using a Monte Carlo method. This method allowed for a statistically rigorous definition of the low, median, and high rates, contrary to the classical upper and lower limits used in most works.

Recognizing the need for updated data and the lack of information close to astrophysical energies, a new measurement of the ^{27}Al(p,α)^{24}Mg reaction has been carried out using the Trojan Horse Method (THM) [11]. Like other indirect methods [12], THM makes it possible to determine astrophysical parameters with no need of extrapolation. Results have been discussed at length in ref.[13, 14], and this work aims to provide a summary, including a comparison with the STARLIB reaction rate library [15] for the ^{27}Al(p,α)^{24}Mg case.

3 The method and the experiment

The ^{27}Al(p,α)^{24}Mg reaction was studied by applying the THM to the $d(^{27}\mathrm{Al}, \alpha^{24}\mathrm{Mg})n$ reaction at 80-MeV ^{27}Al beam energy. A CD_2 target (isotopically enriched to 98%) about 100 μg/cm^2 thick was used to supply the deuterons. In the THM application, deuterons are used to transfer a proton that, under quasi-free (QF) conditions, is the participant to the ^{27}Al(p,α)^{24}Mg reaction while the neutron is emitted without taking part in interaction, so it is labelled as spectator. The QF condition is enforced by gating on small $p-n$ relative momenta, corresponding to $p-n$ relative distances larger than the nuclear interaction radius. Therefore, p and n acts as independent particles strongly simplifying the theoretical formalism.

Under QF conditions and assuming that a single resonance of energy E_R is populated, the THM differential cross section for the $d(^{27}\mathrm{Al}, \alpha^{24}\mathrm{Mg})n$ reaction takes the form [20]:

$$\frac{\mathrm{d}^2\sigma^{\mathrm{TH}}}{\mathrm{d}E_{\alpha^{24}\mathrm{Mg}}\,\mathrm{d}\Omega_{\hat{\mathbf{k}}_{n^{28}\mathrm{Si}}}} = \frac{1}{2\pi}\frac{\Gamma_{\alpha^{24}\mathrm{Mg}}\left(E_{\alpha^{24}\mathrm{Mg}}\right)}{(E_{\alpha^{24}\mathrm{Mg}}-E_R)^2+\frac{1}{4}\Gamma^2(E_{\alpha^{24}\mathrm{Mg}})}\times\frac{\mathrm{d}\sigma_{d(^{27}\mathrm{Al},n)^{28}\mathrm{Si}}}{\mathrm{d}\Omega_{\hat{\mathbf{k}}_{n^{28}\mathrm{Si}}}} \tag{1}$$

where $\dfrac{\mathrm{d}\sigma_{d(^{27}\mathrm{Al},n)^{28}\mathrm{Si}}}{\mathrm{d}\Omega_{\hat{\mathbf{k}}_{n^{28}\mathrm{Si}}}}$ is the differential cross section for the stripping $d(^{27}\mathrm{Al}, n)^{28}$Si to the resonant state of ^{28}Si, $E_{\alpha^{24}\mathrm{Mg}}$ is the $\alpha-{}^{24}$Mg relative energy, Γ and $\Gamma_{\alpha^{24}\mathrm{Mg}}$ are the total and partial width for the resonance under examination. As discussed in ref.[20], a clear connection between the Breit-Wigner approximation for the ^{27}Al(p,α)^{24}Mg cross section and the THM cross section of the $d(^{27}\mathrm{Al}, \alpha^{24}\mathrm{Mg})n$ reaction can be established, making it possible to deduce the resonance strengths $\omega\gamma$ that are the main ingredients, along with the resonance energies, to calculate the reaction rate of a reaction proceeding through narrow resonances [4].

In comparison with ref.[21], data in ref.[13, 14] were taken at a higher beam energy, to explore a phase-space region where the contribution of the ^{25}Mg compound-nucleus decay to the reaction yield is negligible. The experimental setup was made of four 1000-μm double-sided silicon strip detectors (DSSSD), two of them centered at 5.5° and covering each about 4° on opposite sides with respect to the beam direction. The other two (A and D, A on the same side as B) were placed at about 25°, each covering and spanned about 10.5° on opposite sides of the beam axis. No particle identification [23] using, for instance, $\Delta E - E$ measurements, were necessary thanks to the peculiar reaction kinematics.

4 Reaction channel and reaction mechanism selection

Many reactions can be induced in the measurement target due to the presence of carbon and also of contaminants. However, the THM offers the opportunity to carry out accurate channel selection procedures to reduce possible background to negligible values, by making use of the peculiar kinematics of reactions with three particles in the exit channel. While most details can be find in ref.[14], here we mention the use of the energy-momentum plot [23, 24].

In the case of a $a+b \rightarrow c+d+e$ reaction (for instance, the $^{27}\mathrm{Al}+d \rightarrow \alpha+{}^{24}\mathrm{Mg}+n$), the X and Y variables are defined as (assuming that b is the target nucleus, at rest in the laboratory frame):

$$X = \frac{p_e^2}{2u} \qquad Y = E_a - E_c - E_d\,. \tag{2}$$

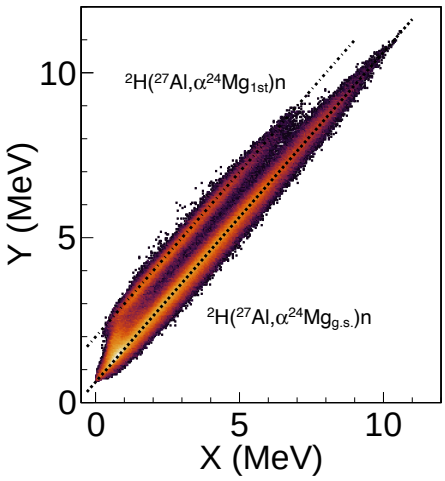

Figure 1. X-Y plot obtained following the procedure in [23, 24] in the laboratory frame. The short-dashed line is used to mark the theoretical locus for the ^{2}H(^{27}Al,α^{24}Mg)n reaction populating ^{24}Mg ground state ($Q_0 = -0.624$ MeV, $A_e = 1$). The dotted–short-dashed line highlights the predicted trend for the feeding of the ^{24}Mg first excited state ($Q_1 = -1.993$ MeV, $A_e = 1$).

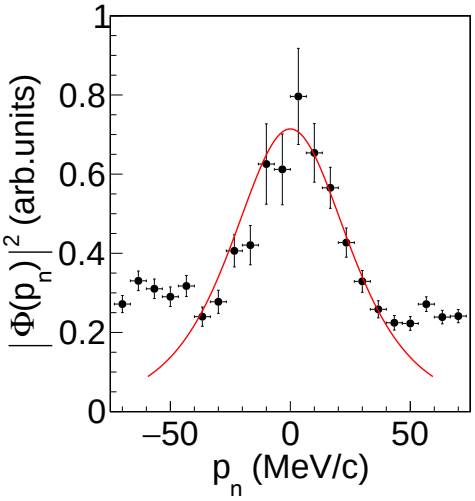

Figure 2. Experimental neutron momentum p_n distribution (solid circles). The theoretical red curve [25] follows very closely the experimental points up to about $|p_n| \leq 40$ MeV/c.

Here, p and E are the momenta and energies of the marked particles and u is the unit mass in a.m.u.. Energy conservation implies that X and Y are linked by the linear equation:

$$Y = \frac{1}{A_e} X - Q \tag{3}$$

where A_e is particle e mass in units of u and Q is the Q-value of the reaction $a + b \rightarrow c + d + e$. Therefore, the intercept on the Y-axis of eq.3 is equal to the Q-value of the reaction with opposite sign and, since p_e is calculated without any assumption on particle e mass [24], the slope is equal to the inverse of the mass of particle e in units of u. Of course, only events for which the energy and momentum conservations laws are satisfied gather along the straight line 3. Other reactions lead to the population of loci well different from a straight line as illustrated in ref.[24].

The X-Y plot representing the current experiment is depicted in fig. 1. The illustration distinctly reveals only two loci, seemingly devoid of any background, instilling confidence in the absence of parasitic processes. Both loci are associated with the ^{2}H(^{27}Al,α^{24}Mg)n reaction. A meticulous examination and comparison with theoretical lines elucidate that events clustering along the short-dashed line correspond to the ^{2}H(^{27}Al,α^{24}Mg)n reaction populating the ^{24}Mg ground state ($Q_0 = -0.624$ MeV, and $A_e = 1$). On the other hand, the locus marked by the dotted-short-dashed line is attributed to the ^{2}H(^{27}Al,α^{24}Mg)n reaction populating the ^{24}Mg 1st excited state at 1.369 MeV ($Q_1 = -1.993$ MeV, and $A_e = 1$). The slopes of the lines distinctly indicate the mass of the undetected particle to be approximately 1 a.m.u., while the intercepts validate the precision of the detector calibration performed.

This analysis and the other ones detailed in ref.[14] show the absence of any observable background, so the investigation of reaction mechanisms leading to the population of the exit channel was conducted. The equations briefly outlined in sec.3 can only be applied under the assumption that the ^{2}H(^{27}Al,α^{24}Mg)n reaction can be described as a QF process. Following the procedure outlined in [14], we examined the relative energy spectra to exclude the presence of sequential decay processes, namely, whether ^{28}Si states are populated in a two-step process. Additional tests, particularly the study of the experimental neutron momentum distribution $|\Phi(p_n)|^2$, were carried out. If the process is direct, neutrons should maintain the same momentum as inside deuterons, and deviation from the theoretical trend [25] would indicate the prevalence of a non-QF reaction mechanism.

The experimental $|\Phi(p_n)|^2$ was obtained following the prescriptions in [25]. The resulting experimental neutron momentum (p_n) distribution is depicted with solid circles in fig. 2, for an $E_{^{24}Mg-\alpha}$ energy window 50-keV-wide centered at 2.2 MeV. Similar results are obtained for other energy values. In the construction of fig. 2, positive or negative sign to p_n was attributed depending on the sign of the cosine of the neutron azimuthal angle $\cos\phi_n$. In this figure, the theoretical $p-n$ relative-momentum distribution is represented with a red solid line, scaled to match the arbitrary normalization of the experimental data. Good agreement is present up to about $|p_n| \leq 40$ MeV/c, as expected (see [14] and references therein). This instills confidence in the occurrence of the QF mechanism in the ^{2}H(^{27}Al,α^{24}Mg)n reaction at 80-MeV beam energy, aligning with findings by [21], suggesting the most suitable cut to introduce in the next steps to single out the QF reaction process.

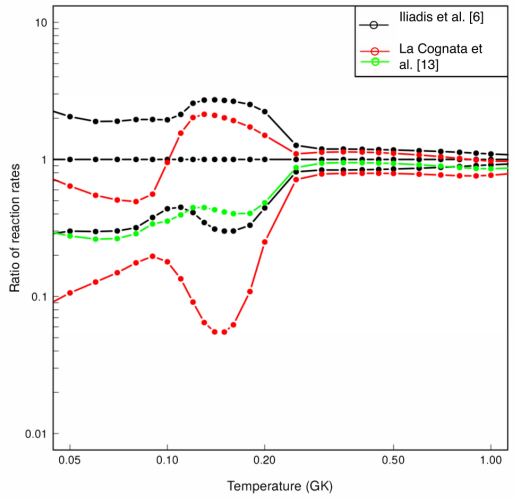

Figure 3. Comparison of THM reaction rate (green line: median rate; red lines: 1σ uncertainty range) with the one listed in the STARLIB compilation [6]. Both median rates and the low/high rates are divided by the STARLIB recommended rate (equal to 1 in this representation).

5 From the resonance strengths to the reaction rate

For the QF events, after angular distribution integration [14], we deduced the ^{2}H(^{27}Al,α^{24}Mg)n cross section and, following the procedures in ref.[14, 20] we deduced the resonances strengths for ^{28}Si states up to about 1.5 MeV above the proton emission threshold. In particular, we could observe a resonance centered at about 84 keV, very important given that the energy region of greatest astrophysical relevance is around 100 keV. High energy resonances, in particular those at 903.54 keV and 1388.8 keV, were used for normalization since: (i) they sit at energies larger than those for which electron screening effects are expected; (ii) they are affected by a comparatively low uncertainty, making it possible to reduce the normalization error; (iii) it has been proved that extending normalization to more than one resonance, a reduction in unpredictable systematic errors affecting direct measurements can be reached [26]. In total, we could determine the resonance strengths of nine resonances and set more stringent upper limits on the strengths of additional three resonances. The resonances strengths deduced in this work are given in tab.1, along with the comparison with ref.[6] strengths. Whenever measured strengths are available in ref.[6], a very good agreement is found with the THM ones, providing a validity test of the method.

For astrophysical applications, the reaction rate of the ^{27}Al$(p,\alpha)^{24}$Mg was computed utilizing the detailed Monte Carlo method implemented in the `RatesMC` code ([6] and references therein). This code offers a statistically robust treatment of uncertainties, incorporating the Porter–Thomas distribution to adequately address upper limits on resonance strengths. Additionally, it employs lognormal probability density for both measured resonance strengths and the overall reaction rate. For the rate calculation, strengths were extracted from tab.1 (columns 6 and 7), while the resonance energies were set to the values reported in ref.[6] (column 2). The comparison of the reaction rate, as depicted in Fig.3, reveals the present-work strengths against the STARLIB values [6]. In this representation, black lines and symbols correspond to literature rates, while the median, low, and high THM rates are represented by green, red, and red lines and symbols, respectively. Despite the persisting uncertainties, particularly above $T_9 \sim 0.1$, where some resonances only have upper limits (albeit lower than those in [6]), a noteworthy outcome is a approximately threefold reduction in the reaction rate, specifically at temperatures relevant to astrophysical scenarios, below $T_9 \sim 0.1$. This might have important consequences for astrophysics that are under examination.

6 Acknowledgements

The author acknowledge the partial support of the European Union - Next Generation EU through the PRIN 2022 project: PRIN_2022RJLWHN, CUP: I53D23000720006

References

[1] Lind, K., et al., Astron. Astrophys. **575**, L12 (2015)
[2] Da Costa, G. S., et al., Astrophys. J. **769**, 8 (2013)
[3] Carretta, E., et al., Astron. Astrophys. **615**, 17 (2018)
[4] Iliadis, C., *Nuclear Physics of Stars* (Wiley-VCH Verlag GmbH & Co, Weinheim, 2015)
[5] Iliadis, C., et al., J. Phys. G: Nucl. Part. Phys. **42**, 034007 (2015)
[6] Iliadis, C., et al., Nucl. Phys. **A841**, 251 (2010)
[7] Groopman, E., et al., Astrophys. J. **809**, 31 (2015)
[8] Angulo, C., et al., Nucl. Phys. **A656**, 3 (1999)
[9] Iliadis, C., et al., Nucl. Phys. **A841**, 31 (2010)
[10] Timmermann, R., et al., Nucl. Phys. **A477**, 105 (1988)
[11] Tribble, R. E., et al., Rep. Progr. Phys. **77**, 106901 (2014)
[12] Torresi, D., et al., Phys. Rev. C **96**, 044317 (2017)
[13] La Cognata, M., et al. , Phys. Lett. B **826**, 136917 (2022)
[14] La Cognata, M., et al. , Astrophys. J. **941**, 96 (2022)
[15] Sallaska, A. L., et al., Astrophys. J. Suppl. Ser. **207**, 18 (2013)
[16] Iliadis, C., et al., Astrophys. J. Suppl. Ser. **134**, 151 (2001)
[17] Endt, P. M., Nucl. Phys. **A521**, 1 (1990)
[18] Endt, P. M., Nucl. Phys. **A633**, 1 (1998)
[19] Endt, P. M., & Booten, J. G. L., Nucl. Phys. **A555**, 499 (1993)
[20] La Cognata, M., et al., Astrophys. J. **708**, 796 (2010)
[21] Palmerini, S., et al., Eur. Phys. J. Plus **136**, 898e (2021)
[22] Champagne, A. E., et al., Nucl. Phys. **A487**, 433 (1988)

Table 1. Spin parities (column 3), strengths and corresponding uncertainties (columns 6 and 7) from ref.[14], compared with the corresponding strengths and errors from ref.[6] (columns 4 and 5). The resonance energies are taken from this latter work (column 2). In column 1 there is a progressive number indexing the resonances. Numbers in italic are upper limits.

N.	$E_{res.}$	J^{π}	$\omega\gamma$ (eV)	$\delta\omega\gamma$ (eV)	$\omega\gamma$ (eV)	$\delta\omega\gamma$ (eV)
(1)	*71.5.*	2^+	$\mathit{2.47 \times 10^{-14}}$	-	$\mathit{8.23 \times 10^{-15}}$	-
(2)	*84.3*	1^-	$\mathit{2.60 \times 10^{-13}}$	-	1.67×10^{-14}	3.2×10^{-15}
(3)	*193.5*	2^+	$\mathit{3.74 \times 10^{-7}}$	-	$\mathit{2.50 \times 10^{-7}}$	-
(4)	*214.7*	3^-	$\mathit{1.13 \times 10^{-7}}$	-	$\mathit{4.36 \times 10^{-8}}$	-
(5)	486.74	2^+	0.11	0.05	0.107	0.021
(6)	609.49	3^-	0.275	0.069	0.245	0.054
(7)	705.08	1^-	0.52	0.13	0.261	0.065
(8)	855.85	3^-	0.83	0.21	0.61	0.35
(9)	903.54	3^-	4.3	0.4	4.20	0.38
(10)	1140.88	2^+	79	27	73	14
(11)	1316.7	2^+	137	47	124	28
(12)	1388.8	1^-	54	15	61	12

[23] Badalà, A., et al., Nuovo Cimento Rivista Serie **45**, 189 (2022)
[24] Costanzo, E., et al., Nucl. Instr. Meth. A **295**, 373 (1990)
[25] Lamia, L., et al., Phys. Rev. C **85**, 025805 (2012)
[26] La Cognata, M., et al., Astrophys. J. **805**, 128 (2015)